Cell

The Bacterial Cytoplasm Has Glass-like Properties and Is Fluidized by Metabolic Activity

Bradley R. Parry,[1,9] Ivan V. Surovtsev,[1,2,9] Matthew T. Cabeen,[1,10] Corey S. O'Hern,[3,4,5] Eric R. Dufresne,[4,5,6,7] and Christine Jacobs-Wagner[1,2,8,*]

[1]Department of Molecular, Cellular, and Developmental Biology, Yale University, New Haven, CT 06520, USA
[2]Howard Hughes Medical Institute, Yale University, New Haven, CT 06520, USA
[3]Department of Applied Physics, Yale University, New Haven, CT 06520, USA
[4]Department of Physics, Yale University, New Haven, CT 06520, USA
[5]Department of Mechanical Engineering and Materials Science, Yale University, New Haven, CT 06520, USA
[6]Department of Chemical and Environmental Engineering, Yale University, New Haven, CT 06520, USA
[7]Department of Cell Biology, Yale University, New Haven, CT 06520, USA
[8]Department of Microbial Pathogenesis, Yale School of Medicine, New Haven, CT 06510, USA
[9]These authors contributed equally to this work
[10]Present address: Department of Molecular and Cellular Biology, Harvard University, Cambridge, MA 02138, USA
*Correspondence: christine.jacobs-wagner@yale.edu
http://dx.doi.org/10.1016/j.cell.2013.11.028

SUMMARY

The physical nature of the bacterial cytoplasm is poorly understood even though it determines cytoplasmic dynamics and hence cellular physiology and behavior. Through single-particle tracking of protein filaments, plasmids, storage granules, and foreign particles of different sizes, we find that the bacterial cytoplasm displays properties that are characteristic of glass-forming liquids and changes from liquid-like to solid-like in a component size-dependent fashion. As a result, the motion of cytoplasmic components becomes disproportionally constrained with increasing size. Remarkably, cellular metabolism fluidizes the cytoplasm, allowing larger components to escape their local environment and explore larger regions of the cytoplasm. Consequently, cytoplasmic fluidity and dynamics dramatically change as cells shift between metabolically active and dormant states in response to fluctuating environments. Our findings provide insight into bacterial dormancy and have broad implications to our understanding of bacterial physiology, as the glassy behavior of the cytoplasm impacts all intracellular processes involving large components.

INTRODUCTION

In eukaryotes, active transport (including ATP-dependent diffusive-like motion) involves protein motors and cytoskeletal filaments. In the absence of cytoskeletal motor proteins, (micrometer-sized) bacteria are thought to primarily rely on diffusion for molecular transport and cytoplasmic mixing. Diffusion is therefore considered an integral part of bacterial life; it determines the mobility of cytoplasmic constituents and hence sets the limits at which molecular interactions (and thereby biological reactions) can occur. Diffusion is also essential for cell proliferation by promoting a homogeneous distribution of cytoplasmic components and the equal partitioning of solutes between daughter cells. Although diffusion in general has been extensively studied theoretically and experimentally, the bacterial cytoplasm bears little resemblance to the simple liquids usually considered. First, the bacterial cytoplasm is an aqueous environment that is extremely crowded (Cayley et al., 1991; Zimmerman and Trach, 1991). Second, the cytoplasm is highly polydisperse, with constituent sizes spanning several orders of magnitude, from sub-nanometer (ions and metabolites) to nanometers (proteins) to tens and hundreds of nanometers (ribosomes, plasmids, enzymatic megacomplexes, granules, and microcompartments) to micrometers (protein filaments and chromosomes). Third, metabolic activities drive the cytoplasm far from thermodynamic equilibrium. Furthermore, as a resistance mechanism, the cell can reversibly shut down metabolism in response to environmental stresses. How these features affect the physical properties of the cytoplasm is poorly understood. Such an understanding is critical because the physical nature of the cytoplasm determines the dynamics of cytoplasmic components and therefore impacts all intracellular processes.

Both normal and anomalous diffusive motions have been reported for cytoplasmic components (Bakshi et al., 2011; Coquel et al., 2013; English et al., 2011; Golding and Cox, 2006; Niu and Yu, 2008; Weber et al., 2010), and a unifying picture about the physical nature of the cytoplasm has yet to emerge. We show here that the bacterial cytoplasm exhibits physical properties typically associated with glass-forming liquids approaching the glass transition. Glass-forming liquids, which are intensively studied in condensed matter physics, encompass

many materials, including molecular glasses (vitreous glass) and dense suspensions of colloidal particles (colloidal glasses) (Hunter and Weeks, 2012). We found that the glassy behavior of the bacterial cytoplasm affects the mobility of cytoplasmic components in a size-dependent fashion, providing an explanation for the previous seemingly conflicting reports. Strikingly, metabolic activity abates this glassy behavior such that, in response to environmental cues, cytoplasmic fluidity and dynamics are dramatically altered through modulation of cellular metabolism.

RESULTS

The Motion of Crescentin-GFP Structures and PhaZ-GFP-Labeled Storage Granules Is Reduced in Metabolically Inactive *Caulobacter crescentus* Cells

Our study began with a serendipitous observation while studying the bacterial intermediate filament protein crescentin. Under native conditions, crescentin self-associates to form a stable (i.e., having no detectable subunit exchange) membrane-bound filamentous structure that generates the namesake curvature of the bacterium *Caulobacter crescentus* (Ausmees et al., 2003). A specific modification of the cell envelope (Cabeen et al., 2010) or addition of a bulky tag (e.g., GFP) to crescentin (Ausmees et al., 2003) causes the crescentin structure to detach from the membrane; these nonfunctional structures display random motion in the cytoplasm (Cabeen et al., 2009). While imaging GFP-labeled crescentin structures in a filamentous mutant strain growing on an agarose pad made with nutrient-containing medium (M2G), we observed, to our surprise, that crescentin-GFP structure movement suddenly stopped when the cells simultaneously arrested growth (Movie S1 available online). The reason for the abrupt growth arrest was unknown, but the ensuing drop in crescentin-GFP structure mobility raised the intriguing possibility that metabolic activity may play a role in the motion of freely diffusing cytoplasmic components.

A possible link between metabolism and cytoplasmic dynamics would be important to investigate, as bacteria in the wild are able to shift between metabolically active and dormant states in response to changing environments (Lennon and Jones, 2011). Dormancy is a survival strategy that can be triggered by many external insults, including nutrient limitation and late stationary phase. To examine whether dormancy can affect cytoplasmic dynamics, we first tracked crescentin-GFP structures (replacing wild-type crescentin structures) in otherwise wild-type cells (using custom two-dimensional tracking methods for non-diffraction-limited objects; see Supplemental Information and Figures S1A–S1F), and compared their mobility in actively growing cells to their mobility in cells subjected to prolonged carbon starvation. In cells actively growing on M2G medium, crescentin-GFP structures displayed motion and were able to sample the cytoplasm in minutes (Figure 1A and Movie S2) by taking large, seemingly random steps (Figure 1B). In contrast, carbon-starved cells were unable to grow, and crescentin-GFP structures rarely left their original locations (Figures 1A and 1B and Movie S3) for the entire duration of the experiment (up to 9 hr; data not shown). We observed similar spatial confinement in late-stationary-phase cells (Figure 1B) and under treatment with 2,4-dinitrophenol (DNP; Figure 1B and Movie S4), an oxidative phosphorylation uncoupling agent that rapidly depletes cells of ATP and GTP.

To quantitatively analyze crescentin-GFP structure mobility at the population level, we calculated the mean square displacement (MSD) over large numbers of trajectories (n = 718–1,943). The MSD averages, over all objects, the square of the distance between an object's current position and its original position (see Supplemental Information). Comparison of one-dimensional (along cell length) MSDs between experimental conditions confirmed the dramatic loss of mobility in metabolically reduced cells (carbon-starved, stationary-phase, and DNP-treated populations; Figure 1C). Thus, the metabolic state of the cell had a dramatic effect on crescentin-GFP structure mobility.

Crescentin-GFP forms large structures, with an average apparent length of 900 nm (Figure S1G). To test whether the motion of other large cytoplasmic components is affected, we tracked the motion of polyhydroxyalkanoate (PHA) granules labeled with PhaZ-mCherry. PhaZ is a PHA depolymerase that binds to PHA storage granules (Maehara et al., 2002; Qi and Rehm, 2001). Consistent with this binding, PhaZ-mCherry formed fluorescent foci (1–2 per cell) that moved inside active (untreated) *C. crescentus* cells (Figure S2A). Metabolic depletion by DNP treatment dramatically reduced motion (Figure S2A), similar to what we observed with crescentin-GFP structures.

Plasmid Motion Is Also Reduced in *Escherichia coli* when Cellular Energy Is Depleted

To examine whether this metabolism-dependent motion is unique to *C. crescentus*, we switched to *E. coli* and examined the motion of engineered low-copy-number mini-RK2 plasmids. These plasmids have an estimated radius of gyration of 150 nm based on measurements of plasmids with similar base-pair lengths (Latulippe and Zydney, 2010). Mini-RK2 lacks a partitioning system and hence is not actively partitioned or constrained in space (Derman et al., 2008). This plasmid also contains a *lacO* array for visualization via GFP-LacI labeling. Mini-RK2 plasmids were imaged every 30 s on agarose pads containing M9-glycerol (M9G) medium to sustain cellular activity. Under these conditions, mini-RK2 plasmids were able to travel the cell length within 1 min, leaving their previous location from frame to frame (Figure 1D and Movie S5), as previously observed (Derman et al., 2008). In contrast, depletion of cellular energy by DNP treatment drastically limited their spatial exploration (Figure 1D and Movie S6), which was confirmed at the population level in MSD plots (Figure 1E; n = 488–497 trajectories). Thus, mini-RK2 plasmids exhibit metabolism-dependent motion in *E. coli*, similar to crescentin-GFP structures and PHA granules in *C. crescentus*. As *E. coli* and *C. crescentus* diverged over one billion years ago, the effect of metabolism on cytoplasmic dynamics is likely to be an ancient and common feature of the bacterial cytoplasm.

Development of a Genetically Encoded Probe to Study Cytoplasmic Dynamics

Specific interactions with other cellular components are known to affect the motion of components endogenous to the cytoplasm, altering motion in an unpredictable manner (Nenninger et al., 2010) and making normal diffusion appear anomalous

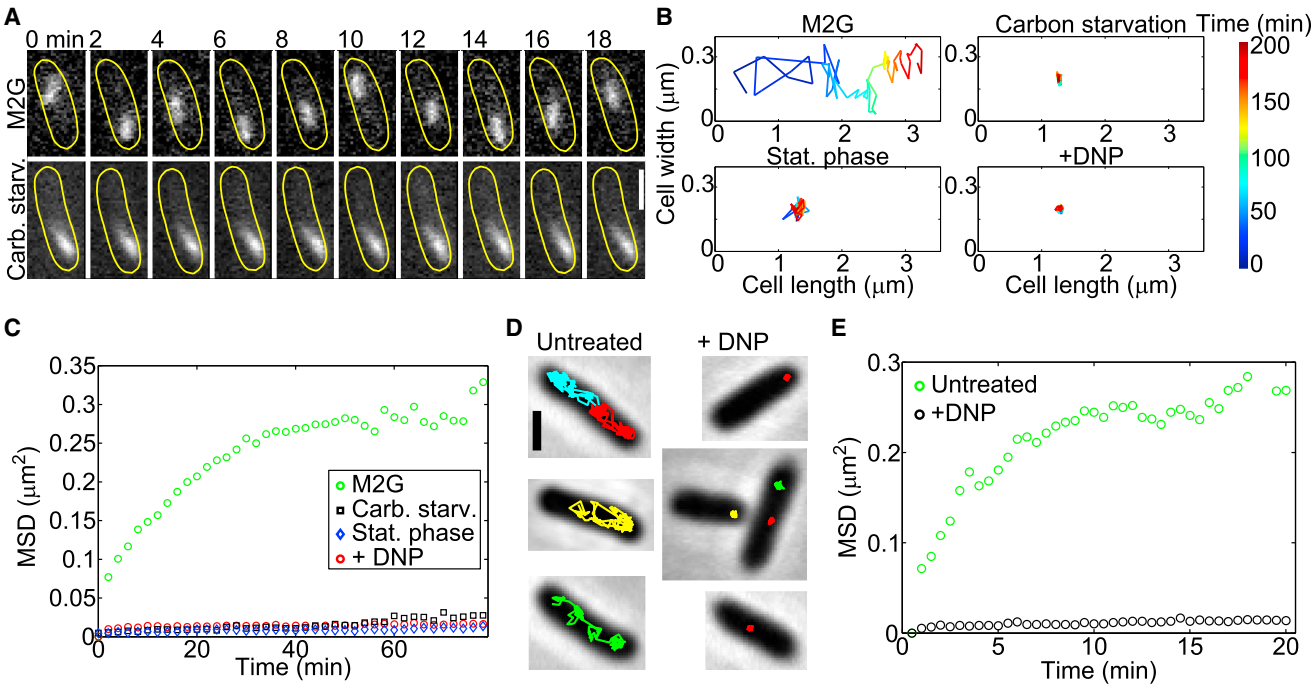

Figure 1. The Mobility of Crescentin-GFP Structures and GFP-LacI-Labeled Mini-RK2 Plasmids Is Affected by Metabolism

(A) Time-lapse montages of crescentin-GFP structures acquired under conditions of growth (M2G) and carbon source depletion. *C. crescentus* cells (CJW1265) were grown and imaged in M2G, a glucose-based medium (top). For carbon starvation, cells were washed into M2 buffer (lacking glucose) and incubated for 3 hr before imaging (bottom). Scale bar, 1 μm.

(B) Two-dimensional trajectories representing 200 min of crescentin-GFP tracking from single *C. crescentus* cells (CJW1265) under metabolically active (M2G) and metabolically depleted (carbon starvation, late stationary phase, + DNP) conditions.

(C) MSD of crescentin-GFP structures in metabolically active (M2G, n = 1,796 trajectories) and energy-depleted (carbon starvation, n = 861 trajectories; stationary phase, n = 718 trajectories; and +DNP, n = 1,943 trajectories) conditions. *C. crescentus* cells (CJW1265) from late stationary-phase cell cultures ($OD_{660} \geq 1.7$) were imaged on agarose pads made with stationary-phase culture supernatant instead of M2G.

(D) Two-dimensional trajectories of GFP-LacI-labeled mini-RK2 plasmids overlaid on corresponding phase-contrast images of metabolically active and DNP-treated *E. coli* cells (JP924). Scale bar, 1 μm.

(E) MSD of mini-RK2 plasmids under metabolically active (untreated, n = 497 trajectories) and energy-depleted (+DNP, n = 488 trajectories) conditions.

See also Figures S1 and S2 and Movies S1–S6.

(Dix and Verkman, 2008). Therefore, to characterize the physical nature of metabolism-dependent motion, we needed a probe that is completely foreign to the cell (unlike crescentin, PHA granules, and plasmids) and is thus unlikely to make any specific interactions with components of the bacterial cytoplasm. As the direct injection methods used in eukaryotic cells cannot be used with micron-sized bacteria, we attempted to introduce nonbiological probes (quantum dots, dextrans, or gold particles) into the bacterial cytoplasm with biolistic and electroporation techniques. None of these attempts were successful. As an alternative, we sought a genetically encoded probe that is foreign to the bacterial cytoplasm and is capable of self-assembly into particles. Several eukaryotic viruses are known to replicate in cytoplasmic factories that require a matrix made of self-assembling viral proteins. The avian reovirus protein μNS is an example of such a self-assembling protein (Broering et al., 2002), and a C-terminal fragment is sufficient to form globular cytoplasmic particles, even when fused to GFP (Broering et al., 2005). These GFP-labeled particles, referred to as GFP-μNS particles here, are unlikely to make specific interactions with components of the bacterial cytoplasm, given the evolutionary divergence between bacteria and the avian reovirus host.

Induction of GFP-μNS synthesis in *E. coli* usually resulted in a single fluorescent focus per cell (Figure S3A). The foci exhibited significant motion in metabolically active cells but became spatially confined with DNP treatment (Figures 2A–2C and Movie S7), recapitulating our results with plasmids, PHA granules, and crescentin-GFP structures. Depletion of cellular energy through treatment with carbonylcyanide-*m*-chlorophenylhydrazone (CCCP) instead of DNP had the same negative effect on GFP-μNS mobility (data not shown). Collectively, these results further support the notion that metabolism-dependent motion is a general property of the bacterial cytoplasm.

Metabolism-Dependent Motion Is Not Driven by Known Motor-like Activity or Chromosome Dynamics

The observation that the motion of cytoplasmic components depends on metabolic activity was surprising, as it appeared inconsistent with diffusion, which is a passive process. ATP-dependent motion was recently reported for chromosomal loci in *E. coli* (Weber et al., 2012). However, chromosomal loci are

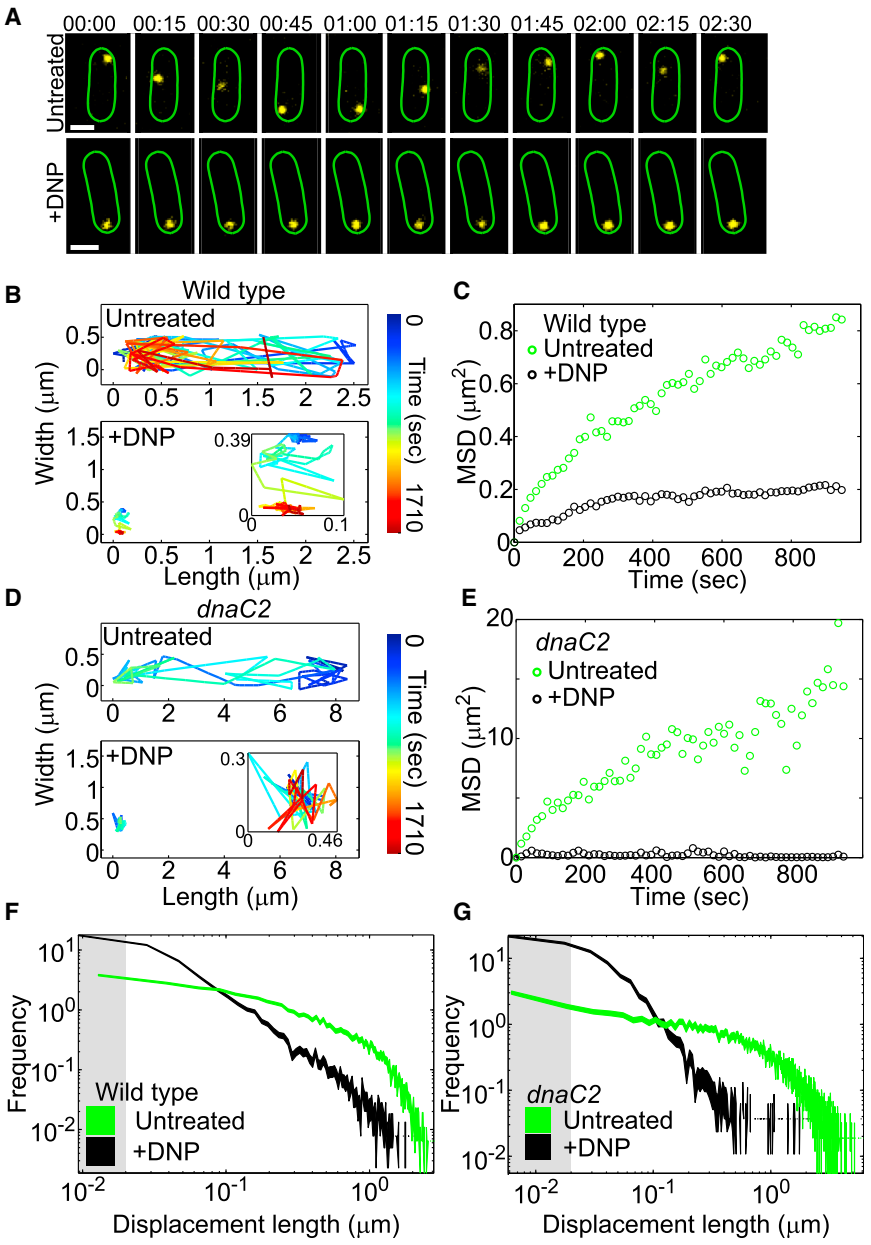

Figure 2. GFP-μNS Probe Dynamics Are Affected by Cellular Metabolism

(A) Representative time-lapse montages of GFP-μNS particles (yellow) in *E. coli* cells (CJW4617) acquired under untreated and DNP-treated conditions (+DNP). Scale bar, 1 μm. Time is min:sec.

(B) An example of a two-dimensional trajectory of a GFP-μNS particle in an *E. coli* cell (CJW4617), with or without DNP treatment.

(C) MSD of GFP-μNS particles in metabolically active (untreated, n = 729 trajectories) and DNP-treated (+DNP, n = 643 trajectories) *E. coli* cells (CJW4617).

(D) Two-dimensional trajectory of a GFP-μNS particle in a filamentous *E. coli dnaC2* cell (CJW4619) at the restrictive temperature (37°C) with or without DNP treatment.

(E) MSD of GFP-μNS particles in filamentous *E. coli dnaC2* cells (CJW4619) at their restrictive temperature with (+DNP, n = 118 trajectories) or without (untreated, n = 192 trajectories) DNP treatment.

(F) Histogram of GFP-μNS particle displacements in *E. coli* cells (CJW4617) with or without DNP treatment. Line width indicates Poisson counting error, and the gray shading delineates the estimated tracking error. Displacements were measured over 15 s intervals.

(G) Histogram of GFP-μNS particle displacements in *E. coli dnaC2* cells (CJW4619) at the restrictive temperature (37°C) with or without DNP treatment. Line width indicates Poisson counting error, and the gray shading delineates the estimated tracking error. Displacements were measured over 15 s intervals.

See also Figures S2–S5 and Movie 7.

distinct from free cytoplasmic components, as they remain confined within a small space (where they "jiggle") by virtue of their attachment to the rest of the chromosome. As a consequence, the motion of chromosomal loci depends not only on the cytosolic environment, but also on the DNA structure. Using DAPI staining, we found that energy depletion by DNP treatment has a strong effect on the shape and hence the structure of the chromosome (Figures S4A and S4B) and likely contributes to the change in chromosomal locus dynamics. Consistent with this notion, the mobility of chromosomal loci is also ATP dependent in eukaryotic nuclei (Heun et al., 2001; Levi et al., 2005), and this ATP dependence has been attributed to reduced activity of DNA-remodeling proteins (Soutoglou and Misteli, 2007).

Although our cytoplasmic probes do not associate with the chromosome, it remained possible that their metabolism-dependent motion results from a change in chromosome structure and dynamics (for example, through probe entrapment; see Supplemental Information). We found that the chromosome affected the spatial distribution of GFP-μNS particles (see Supplemental Information). However, experiments with *dnaC2* mutant cells, which produce large DNA-free regions, showed that metabolism-dependent motion occurs independently of the DNA (see Supplemental Information and Figures 2D, 2E, and S2B). These experiments exclude a predominant role for the chromosome in the metabolism-dependent motion of free cytoplasmic components.

In eukaryotes, agitation of the pervasive cytoskeletal meshwork by the activity of motor proteins can produce diffusive-like motion in the cytoplasm in an ATP-dependent manner (Brangwynne et al., 2009). This process is often referred to as "active diffusion." However, bacteria lack motor proteins like dyneins, myosins, and kinesins, and their cytoskeletal elements are primarily membrane associated. Furthermore,

metabolism-dependent motion still occurred when the polymerization of MreB (bacterial actin homolog) or FtsZ (tubulin homolog) was disrupted (see Supplemental Information and Figures S3B, 2E, 2D, and S2B note that FtsZ rings do not form in filamentous *dnaC2* cells). Thus, the mechanism producing the metabolism-dependent motion in bacteria appears different from the cytoskeletal motor-based "active diffusion" observed in eukaryotes.

Through drug inactivation of transcription, translation, or peptidoglycan wall synthesis, we also showed that metabolism-dependent motion does not originate from the sole (motor-like) action of RNA polymerases, ribosomes, or penicillin-binding proteins on their DNA, mRNA, or peptidoglycan substrates (see Supplemental Information and Figures S3C–S3E).

Increase in Frequency of Large Displacements Contributes to Metabolism-Dependent Motion

To gain insight into the origin of metabolism-dependent motion, we sought to characterize this motion more precisely. An interesting characteristic of energy-depleted cells is that, although GFP-μNS particles remained largely confined in space in these cells, they still appeared to display small displacements over the imaging interval (15 s); this was true in wild-type and *dnaC2* cells (see Figures 2B and 2D for example trajectories). Through control experiments and simulations (see Supplemental Information and Figure S5), we determined that our single-particle tracking method can distinguish small (>20 nm) displacements. Therefore, even after accounting for potential localization errors, GFP-μNS particles displayed discernible motion in DNP-treated cells, as shown by the distributions of displacement lengths (Figure 2F for wild-type cells and Figure 2G for *dnaC2* cells, with gray shading denoting our estimated tracking error; see Supplemental Information). Under both untreated and DNP-treated conditions, small displacements were more frequent than large ones (Figures 2F and 2G). However, the frequency of long displacements was much greater in metabolically active cells. This higher frequency of long displacements is likely responsible for the ability of GFP-μNS particles to explore more cytoplasmic area in active cells. In other words, GFP-μNS particles are able to sample the cytoplasm of active cells with large displacements, though they remain spatially confined in inactive cells because the largest displacements disappear.

The Effect of Metabolism on Cytoplasmic Dynamics Depends on Particle Size

Recent fluorescence recovery after photobleaching (FRAP) measurements from our laboratory have shown only a nominal difference in the diffusion coefficient of free GFP between untreated and DNP-treated *C. crescentus* cells (Montero Llopis et al., 2012). Because GFP (size ≈3 nm) is smaller than mini-RK2 plasmids, PHA granules, and crescentin-GFP filaments, this observation raised the possibility that the influence of metabolism on motion may depend on particle size. To examine this possibility, we took advantage of our titratable GFP-μNS system in which GFP-μNS synthesis can be tuned to different levels by varying the inducer (IPTG) concentration and the induction time. By doing so, we obtained GFP-μNS particles with a wide range of fluorescence intensities and hence sizes (Figure S6A and S6B). We then plotted MSDs of particles binned by fluorescence intensities (bins 1–9) and found that MSDs of both untreated and DNP-treated cell are inversely correlated with fluorescence intensity (Figures 3A and 3B show selected bins on a log-log scale for clarity), as anticipated. When we compared the distribution of displacement lengths between untreated and DNP-treated conditions across discrete bins of particle fluorescence intensities, we found that the difference between the two conditions is accentuated with fluorescence intensity and hence particle size (Figures 3C and S7).

To estimate the absolute size of particles from their fluorescence intensity, we measured the diffusion coefficients of GFP-μNS particles in solution after cell lysis and compared these values to those of fluorescent beads of known size (see Supplemental Information and Figures S6C and S6D). From these measurements, we obtained a calibration curve (see Supplemental Information), which we used to estimate the particle size (in nm). We then characterized the relationship between particle size and metabolism-dependent motion by calculating the radius of gyration (R_g; along the long axis of the cell) of each trajectory. R_g is the root-mean-square distance from the center of the trajectory (see Supplemental Information) and measures the average space that a particle explores. R_g analysis showed that both cellular energy depletion (+DNP) and increasing particle size leads to increasing spatial confinement (Figure 3D). By calculating the ratio $(R_g^{untreated} - R_g^{+DNP})/R_g^{+DNP}$ (which compares the difference in space explored in metabolically active conditions relative to energy-depleted conditions) as a function of particle size (Figure 3E), we found that the ratio is significantly greater than zero and increases with increasing particle size (except perhaps for the largest size bin, possibly because these particles may be too big to move even in active cells). This trend supports a size dependence for metabolism-dependent motion. Of equal interest, the ratio $(R_g^{untreated} - R_g^{+DNP})/R_g^{+DNP}$ decreased toward 0 as size decreased (Figure 3E), with an estimated intercept near 30–40 nm assuming a linear relationship. This finding suggests that cytoplasmic components smaller than this estimated size are not affected by metabolism-dependent motion.

The Distribution of Displacements Is Non-Gaussian

In normal diffusion, the diffusing particles will exhibit a Gaussian distribution of displacements. In contrast, the displacement distributions of GFP-μNS particles under both untreated and DNP-treated conditions diverged from the expected Gaussian distribution (Figure 4A shows bin 5 as an example), as signified by long tails. We quantified deviations from a Gaussian distribution by calculating the non-Gaussian parameter α_2 (see Supplemental Information). The α_2 value of a Gaussian distribution is zero and grows as the tail of the measured distribution increases. First, we found that, in metabolically active cells, the α_2 values of GFP-μNS displacement distributions grew with increasing GFP-μNS particle size (Figure 4B), indicating that non-Gaussian behavior increases with particle size. Second, the non-Gaussian behavior was dramatically stronger for particles in metabolically inactive cells, wherein α_2 grew much faster with particle size than in active cells (Figure 4B).

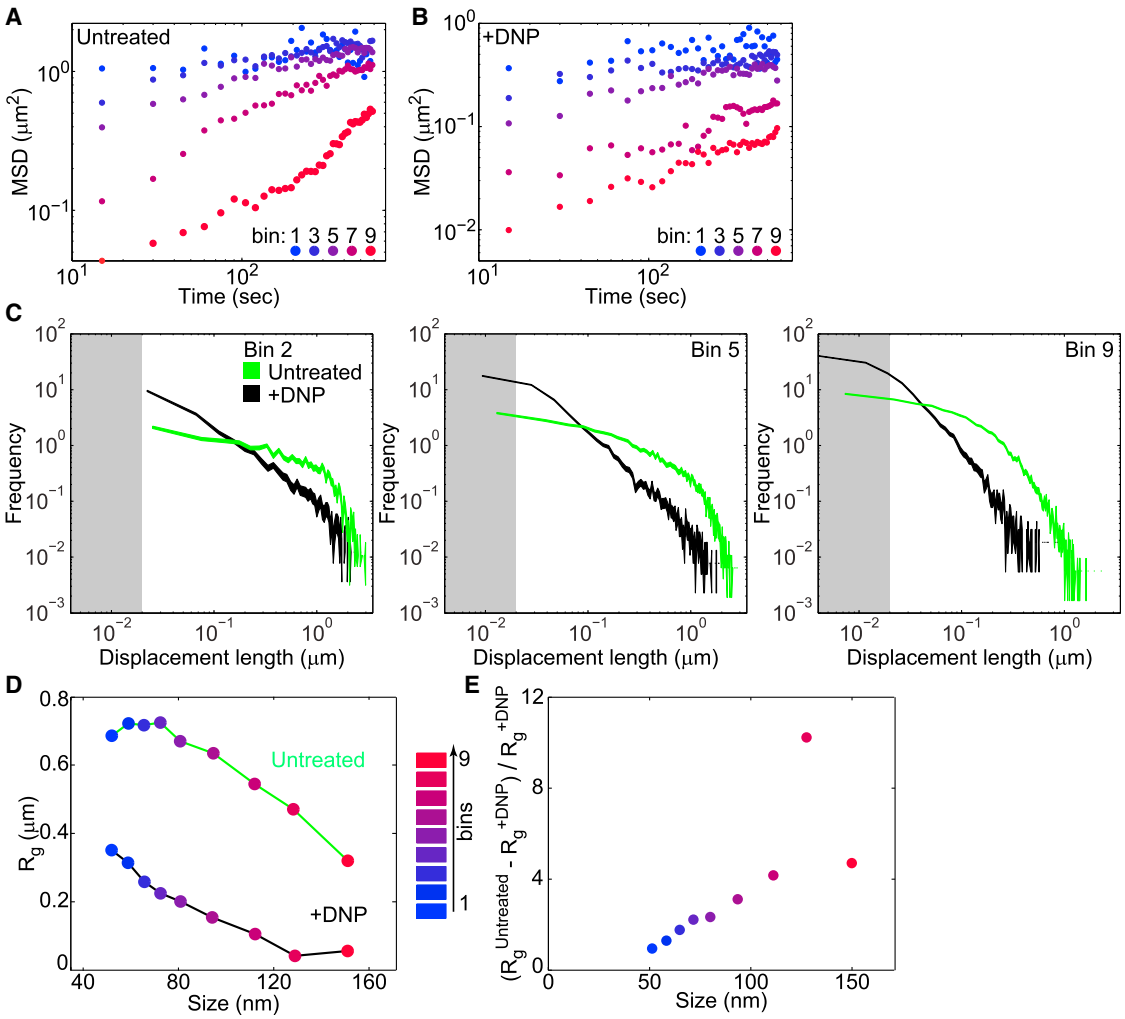

Figure 3. Effect of Metabolism on Cytoplasmic Motion Depends on Particle Size

(A) MSD of GFP-μNS particles of varying binned fluorescence intensities in *E. coli* cells (CJW4617) under normal growth conditions (M2G).

(B) Same as (A) but for GFP-μNS particles in *E. coli* cells (CJW4617) under DNP treatment.

(C) Histograms of GFP-μNS particle displacements under untreated and DNP-treated conditions for selected bins. Displacements were measured over 15 s intervals. Line width indicates Poisson counting error, and the gray shading delineates the estimated tracking error.

(D) Mean radius of gyration (R_g) of all trajectories from GFP-μNS particles of a given binned size is plotted as a measure of spatial exploration for untreated and DNP-treated cells.

(E) The ratio $(R_g^{untreated} - R_g^{+DNP})/R_g^{+DNP}$ is plotted as a function of particle size.

See also Figures S6 and S7.

Nonergodicity Increases with Energy Depletion and Particle Size

Notably, deviations from Gaussian statistics for particle displacements have been reported in various nonliving physical systems, including glass-forming liquids near the glass transition. Colloidal suspensions have proven to be instructive model systems to characterize the dynamics of glass-forming liquids (Hunter and Weeks, 2012). Dense colloidal suspensions (also known as colloidal glasses) are metastable near the glass transition, changing from liquids to amorphous solids with small changes in colloid concentration. At low concentration (low crowding), colloidal particles exhibit diffusive behavior. Increasing the concentration of particles results in a strong increase in viscosity and a decrease in particle mobility, ultimately driving the system through the glass transition to a disordered solid-like state (Pusey and van Megen, 1986). The approach to the glass transition is accompanied by several distinct features. For example, the non-Gaussian parameter α_2 increases as the system approaches the glass transition (Kegel and van Blaaderen, 2000; Marcus et al., 1999; Weeks et al., 2000). Additionally, the system becomes nonergodic (Cipelletti and Ramos, 2005). In ergodic systems, time averages are equivalent to ensemble averages. For example, to measure probe diffusion in cells, one could either track a probe in a single cell over a very long time and average over all times or track many probes in different cells over a short time and average over all probes. The two methods produce the same

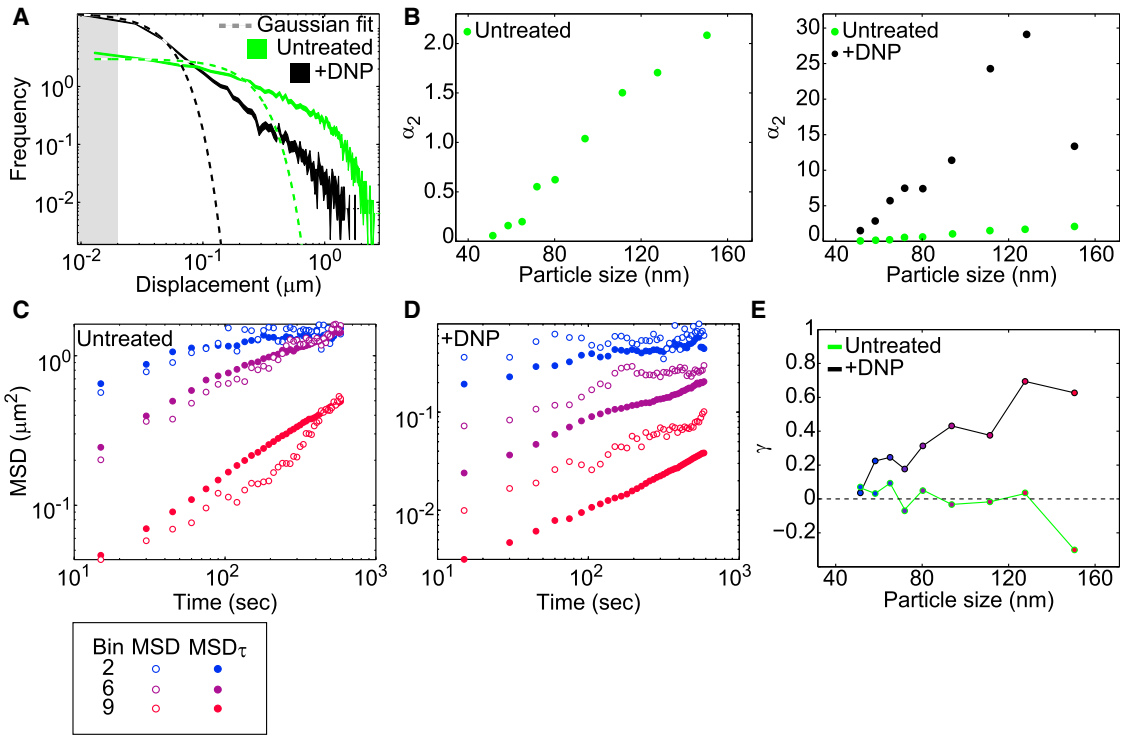

Figure 4. GFP-μNS Particles Display Non-Gaussian and Nonergodic Behavior in the Cytoplasm

(A) Experimental distributions of GFP-μNS particle displacements for *E. coli* cells (CJW4617) under untreated and DNP-treated conditions for a selected size bin (bin 5). Dashed lines are the best fit to a Gaussian distribution. Line width indicates Poisson counting error, and the gray shading delineates the estimated tracking error. Time interval is 15 s.

(B) Non-Gaussian parameter α_2 of particle displacement distributions is plotted as a function of particle size for *E. coli* cells (CJW4617) with or without DNP treatment.

(C) Comparison of MSD and MSD_τ for selected size bins for cells under untreated conditions.

(D) Same as (C) but for cells under DNP treatment.

(E) The parameter γ is plotted as a function of particle size for cells with or without DNP treatment.

result if the system is ergodic. Nonergodicity can arise from caging or aging phenomena, whereby the probe becomes trapped in a given region or the system slowly moves from one region of configuration space to another.

If the cytoplasm were ergodic, we would expect ensemble-averaged MSDs of many GFP-μNS trajectories to coincide with the time-averaged MSD of a single trajectory. Obtaining the time-averaged MSD of a trajectory in a single cell with sufficient statistics for this comparison requires acquisition of an extremely long trajectory, which was not possible for GFP-μNS particles due to technical limitations (photobleaching and phototoxicity). Instead, we compared ensemble-averaged MSDs with an MSD (MSD_τ) that is both time and ensemble averaged (see Supplemental Information). If the system were ergodic, MSD and MSD_τ would be equivalent. We found relatively close agreement between the MSD and its corresponding MSD_τ for GFP-μNS particles in untreated cells (Figure 4C), except perhaps for the largest particles. However, in DNP-treated cells, MSD and MSD_τ were significantly different for all particle sizes, and this difference was greatest for the largest GFP-μNS particles (Figure 4D). We defined a parameter γ to measure the difference between the MSD and MSD_τ (see Supplemental Information), with $\gamma = 0$ indicating equivalency between MSD and MSD_τ. For GFP-μNS particles in metabolically active cells, γ fluctuated near zero except for GFP-μNS particles of the largest size bin (Figure 4E). However, under metabolic depletion, γ grew in response to increasing GFP-μNS particle size (Figure 4E). These differences cannot be explained by the finite number of trajectories or by their limited duration (see Supplemental Information). These results suggest that the bacterial cytoplasm becomes increasingly nonergodic with both energy depletion and increasing particle size.

The Cytoplasm Displays Dynamic Heterogeneity

Although non-Gaussian statistics and ergodicity breaking are consistent with glassy dynamics, a hallmark of glassy systems is dynamic heterogeneity, which is characterized by regions of high particle mobility coexisting with regions of low particle mobility (Berthier, 2011). Due to crowding, particles in colloidal suspensions can become trapped by their nearest neighbors, resulting in small random displacements of the particles. Over longer times, the "cage" formed by their neighbors can spontaneously rearrange through collective motion, allowing the particles to escape with large displacements. Particles in regions

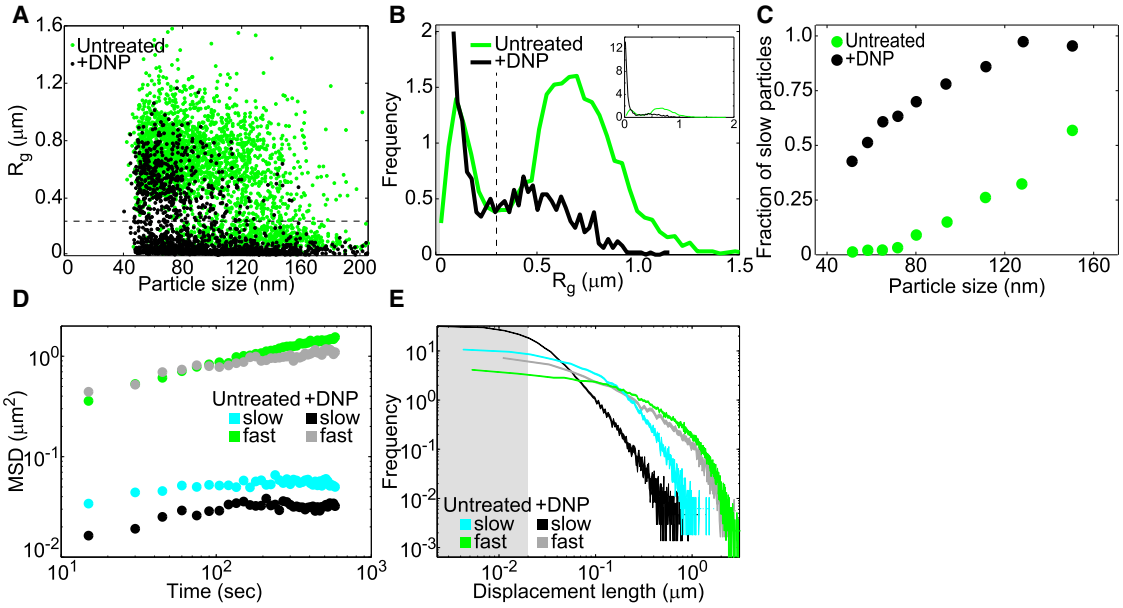

Figure 5. Two Subpopulations of GFP-μNS Particles Exist in Both Active and Inactive Cells

(A) Radius of gyration (R_g) of individual trajectories is plotted as a function of GFP-μNS particle size for *E. coli* cells (CJW4617) under untreated and DNP-treated conditions. The horizontal dashed line delimits slow (R_g < 0.3 μm) and fast (R_g > 0.3 μm) particles.

(B) Histogram of R_g for cells under untreated and DNP-treated conditions. The vertical dashed line delimits slow (R_g < 0.3 μm) and fast (R_g > 0.3 μm) particles. The gray shading delineates the estimated tracking error.

(C) Fraction of slow particles (R_g < 0.3 μm) for trajectories in each size bin for cells with or without DNP treatment.

(D) MSD of slow (R_g < 0.3 μm) and fast (R_g > 0.3 μm) GFP-μNS particles.

(E) Distribution of displacements for slow (R_g < 0.3 μm) and fast (R_g > 0.3 μm) GFP-μNS particles under untreated and DNP-treated conditions. The line width indicates Poisson counting error, and the gray shading delineates the estimated tracking error.

with different cage rearrangement times will exhibit different dynamics.

To examine whether heterogeneity in particle dynamics exists in the GFP-μNS tracking experiments, we plotted R_g measurements of individual GFP-μNS trajectories as a function of particle size (Figure 5A). Interestingly, the R_g values split GFP-μNS particles into two distinct subpopulations at an R_g value of 0.3 μm, irrespective of particle size or metabolic state of the cell. This can be easily seen in the distributions of R_g (Figure 5B). Because R_g is a measure of how much space a particle explores on average, we will refer to the two populations as "slow" (R_g < 0.3 μm) and "fast" (R_g > 0.3 μm) particles. Though fast and slow particles were found in both active and inactive cell populations, their fraction differed, with the fraction of slow particles being low in the active (untreated) cell population and high in the inactive (+DNP) cell population (Figure 5B). This trend was observed across the nine bins of particle sizes (Figure 5C). Thus, the fraction of slow and fast particles appears to be the primary reason for the difference in dynamics between active and inactive cells. Note that the presence of fast particles in the DNP-treated cell population was not due to cell growth by DNP-resistant cells, as no DNP-treated cells (out of 4×10^9 cells) were able to form a colony after overnight incubation.

The slow and fast particle populations from both active and inactive cells exhibited markedly different behavior, as evident from their MSDs (Figure 5D) and displacement distributions (Figure 5E). Fast particles not only explored more cytoplasmic space on average but did so with displacements from distributions shifted toward longer lengths. Most striking was the observation that fast particles from both untreated and DNP-treated conditions behave similarly, with virtually overlapping MSDs and displacement length distributions (Figures 5D and 5E). Although not to the same degree, the behavior of slow particles was also close between metabolically active and energy-depleted conditions. This suggests that particles from the fast population and, to a lesser extent, particles from the slow population experience a similar local environment regardless of metabolic status.

The difference in particle dynamics (slow and fast) may reflect dynamic heterogeneity within the cytoplasm. Similar to glass-forming liquids, the slow particles would be caged by neighboring macromolecules and have a low probability of escape, whereas the probability of escape through collective rearrangement of neighboring macromolecules would be greatly increased for fast particles. The collective effect of all ongoing metabolic activities in active cells would facilitate cage turnover, which would explain the observed higher fraction of fast particles in active cells (Figures 5B and 5C). Alternatively, the two populations in particle dynamics may stem from heterogeneity among cells: some cells would have slow particles, whereas others would have fast particles. In this latter case, two particles in the same cell would always behave similarly (slow or fast), whereas in the first scenario (heterogeneity within the cytoplasm), slow and fast dynamics could coexist in a single cell. To test this, we sought to identify instances of cells containing

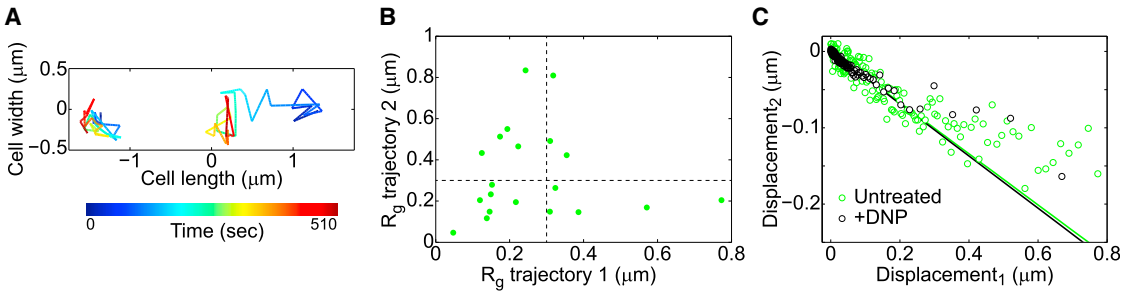

Figure 6. Double-Particle Tracking and Correlation of Displacements Are Consistent with Dynamic Heterogeneity in the Cytoplasm

(A) Example of two-dimensional trajectories of two GFP-μNS particles in a single *E. coli* cell (CJW4617). The trajectory of the left particle has a radius of gyration R_g = 0.12 μm, and the particle has an estimated size d = 144 nm; for the right particle, R_g = 0.43 μm and d = 158 nm.

(B) Radius of gyration (R_g) of individual trajectories for pairs of GFP-μNS particles in individual *E. coli* cells (CJW4617) under metabolically active conditions. Only the results for particle pairs with a difference of particle size of less than 10% are shown. The horizontal dashed line delimits slow (R_g < 0.3 μm) and fast (R_g > 0.3 μm) particles.

(C) Plot showing the average displacement length (displacement$_2$) following an initial displacement (displacement$_1$) of a given length for GFP-μNS particles in *E. coli* cells (CJW4617) under untreated and DNP-treated conditions. The second displacement was signed positive if it was in the same direction as the initial displacement and negative otherwise. Each point represents the average of 700 displacements. Solid lines represent the best fit (displacement$_2$ = −0.34 displacement$_1$) to the data where displacement$_1$ < 0.2 μm. The time interval is 15 s.

two particles of similar size (within 10%). Cells with two GFP-μNS foci were rare and tended to be observed only under greater induction conditions of GFP-μNS synthesis, which led to larger and thus slower particles. Despite the bias toward slower particles, we still found that fast (R_g > 0.3 μm) particles could coexist with slow (R_g < 0.3 μm) particles (Figures 6A and 6B), arguing that the difference in dynamics primarily comes from dynamic heterogeneity within the cytoplasm of individual cells.

Local Caging Is Mitigated by Cellular Metabolism

In dense colloidal suspensions, local caging is evident in correlation analysis of consecutive displacements (Doliwa and Heuer, 1998; Weeks and Weitz, 2002). For small displacements, the local caging results in a negative linear correlation between consecutive displacements. The linear relationship does not hold for longer displacements, which indicates the escape of the particle from its cage, presumably through collective rearrangement of its neighbors. To examine whether the dynamics of GFP-μNS particles are linked to caging, we calculated the average displacement length following an initial displacement of a given length (signed positive if the second displacement was in the same direction as the initial displacement and negative otherwise). An object trapped in a container with perfectly reflecting walls exhibits an apparent negative correlation between two subsequent steps with a correlation coefficient c = −0.5 (Doliwa and Heuer, 1998). If the object has a nonzero probability of escaping the cage, the correlation coefficient is expected to be between 0 and −0.5. For small initial displacements (<200 nm), we observed a strong negative correlation (c = −0.34 for both untreated and DNP-treated cells; Figure 6C), in agreement with local caging. Around 250 nm, this linear relationship breaks, consistent with cage escape. The break in linearity provides an estimation of the cage size (Weeks and Weitz, 2002). The higher number of displacements above 250 nm in untreated cells rather than in DNP-treated cells (reflected by the greater number of data points greater than 250 nm in Figure 6C) suggests more frequent cage escape and thus higher cage turnover under metabolically active conditions, consistent with the greater proportion of fast particles in the active cell population (Figures 5B and 5C). This result suggests that cellular metabolism facilitates long-distance motion by increasing cage rearrangement (see Discussion).

DISCUSSION

Our findings fundamentally alter the way that we view the bacterial cytoplasm. We show that, above a certain size scale (~30 nm), the bacterial cytoplasm behaves differently from a simple (viscous) fluid. Instead, it displays striking features (such as non-Gaussian distributions of displacements with long tails, nonergodicity, caging, and dynamic heterogeneity; Figures 4B, 4E, 5A, and 6) that are characteristic of colloidal glasses (Cipelletti and Ramos, 2005; Hunter and Weeks, 2012). The cytoplasm behaves as a liquid for small particles while it increasingly behaves as a glass-forming liquid approaching the glass transition with increasing particle size. This size dependence provides an explanation for previous seemingly conflicting reports of normal and anomalous diffusion (see Supplemental Information and Figures S6E–S6G). In dense colloidal suspensions containing particles of two sizes, the smaller particle can be mobile, perceiving the environment as a liquid, while the larger one can display glassy dynamics (Zaccarelli et al., 2005). This is in line with the size-dependent dynamics that we observed for GFP-μNS particles. As their size increases, GFP-μNS particles would become increasingly constrained by other surrounding components of the cytoplasm.

Remarkably, the glassy dynamics are partially suppressed by metabolic activity in a size-dependent manner. In other words, our data suggest that cellular metabolism enhances the motion of cytoplasmic components by "fluidizing" the cytoplasm, and this effect increases with component size.

What Is the Origin of the Glassy Behavior?

Aspects of glassiness have been reported in eukaryotic cells but have been attributed to the mechanical response of their

extensive cytoskeletal network (Fabry et al., 2001). Bacteria lack such a pervasive cytoskeletal meshwork and its associated motors. However, the bacterial cytoplasm is more similar to colloidal glasses by being more crowded than the eukaryotic cytoplasm based on the diffusion coefficient of free GFP being about three times smaller in *E. coli* than in eukaryotic cells (Elowitz et al., 1999; Swaminathan et al., 1997). Because crowding in dense colloidal suspensions is responsible for their glassy dynamics, it is likely that the glassy behavior of the bacterial cytoplasm originates from its extreme crowding (Cayley et al., 1991; Zimmerman and Trach, 1991). While measuring crowding inside bacterial cells is technically difficult and is subject to uncertainties, estimates suggest that macromolecules occupy 20%–40% of the bacterial cytoplasm (Cayley et al., 1991; Zimmerman and Trach, 1991). An additional ~20% of the cytoplasm consists of "bound" water, presumably as a hydration layer to macromolecules (Cayley et al., 1991), suggesting that the total excluded volume may range between 40%–60%. Colloidal suspensions can exhibit glassy dynamics over a wide range of volume fractions depending on the properties of the system. For example, monodisperse suspensions of noninteractive colloidal particles vitrify at volume fractions near 58% (Hunter and Weeks, 2012). Importantly, elements of glassy dynamics are observable at lower (e.g., 45%) volume fractions (Kegel and van Blaaderen, 2000; Weeks et al., 2000). If the colloidal particles are interacting, glassy dynamics can occur at even lower volume fractions (Dawson, 2002). Furthermore, glass transition occurs at a lower density in a confined geometry (Fehr and Löwen, 1995).

How Can Cellular Metabolism Fluidize the Cytoplasm to Enhance Motion?

The nucleoid affects the distribution of large components (Coquel et al., 2013), and the dynamics of individual chromosomal loci change with ATP depletion (Weber et al., 2012). However, we found that metabolic depletion results in the confinement of both GFP-μNS particles and mini-RK2 plasmids, even when they are located in the large DNA-depleted regions of filamentous *dnaC2* cells (Figures 2D, 2E, and S2B). Thus, DNA dynamics, DNA-related processes (e.g., transcription), or agitation of the DNA mesh from DNA-associated activities cannot be the driving factor underlying metabolism-dependent motion and the proposed increase in cage turnover in active cells. We also ruled out a predominant role for MreB (Figure S3B) or FtsZ (Figures 2D, 2E, and S2B; note that filamentous *dnaC2* cells do not make FtsZ rings). Inhibiting translation or peptidoglycan synthesis had little, if any, measurable effect on metabolism-dependent motion (Figures S3C and S3E). This suggests that any of these processes cannot alone account for the observed metabolism-dependent motion. However, there are a multitude of cellular processes occurring simultaneously inside of metabolically active cells. We envision that these processes collectively promote cage turnover, as opposed to a single process being solely responsible.

How could cellular activities collectively increase cage turnover? Spitzer and Poolman argued that, from a physical chemistry perspective, hydrophobic and screened electrostatic interactions, together with macromolecular crowding, must result in the formation of overcrowded regions of macromolecules separated by a more fluid phase of less-crowded cytosol (nanopools) (Spitzer, 2011; Spitzer and Poolman, 2009). Their theory also stipulates that metabolic reactions, by altering the hydrophobicity and charge of molecules, would continuously remodel the topology of nanopools and overcrowded regions within the cytoplasm. Following this view, it is conceivable that large particles would become caged in the overcrowded regions or nanopools and that the metabolism-dependent rearrangement of these domains would promote their long-range motion. A second, nonexclusive way by which metabolism could promote cage turnover does not require microphase separation and is based on the notion that cellular activities cause agitations to the system. A remarkable property of liquids near a glass transition is that small changes in the system can dramatically modify its fluidity. In a colloidal glass, particles are caged by surrounding neighbors. However, agitation can fluidize the system by increasing the rate of cage rearrangements (Petekidis et al., 2002). We provide evidence that cellular metabolism promotes cytoplasmic fluidization (Figures 1, 2, 3, 4, and 5) and uncaging (Figure 6C). Metabolic activity can cause a variety of perturbations (conformational changes, fluid displacements, nonequilibrium fluctuations, etc.) that may collectively influence cage rearrangement, allowing cage escape and long-distance motion. When all metabolic activities are abolished, rearrangement of the local domain (cage) would become rare (as in nonliving glassy materials), leading to particle confinement.

What Are the Biological Implications?

Current models of bacterial processes generally consider the cytoplasm as a simple fluid. However, even in active cells, the cytoplasm retains glassy features in a component-size-dependent manner (Figures 4B, 5A–5C, and 6C). Based on our rough critical size estimation, we expect that cytoplasmic constituents $\geq$30 nm will be subject to metabolism-dependent motion. This implies that proteins, which typically have a size <10 nm, will not be affected, consistent with the minimal effect of DNP on the apparent diffusion of free GFP in *C. crescentus* (Montero Llopis et al., 2012). However, larger cellular components such as plasmids (Figures 1D and 1E), protein filaments (Figures 1A–1C), storage granules (Figure S2A), and the multitude of other large components populating the cytoplasm (e.g., polyribosomes, chromosomes, enzymatic megacomplexes, intracellular organelles, phage capsids and genomes, microcompartments, etc.) will be impacted by the glassy behavior of the cytoplasm and the metabolic state of the cell. Many of these large components are involved in processes that are essential for life and fitness in natural environments, and their functions depend on their ability to move in the cytoplasm. For example, although the origin region of the chromosome segregates via an active mechanism, the bulk of the chromosome has been proposed to partition passively through an entropy-driven mechanism (Jun and Wright, 2010) that implies diffusion. Similarly, multicopy plasmids and some storage granules require motion for their partitioning (which is essential for their propagation). Low-copy plasmids typically have a dedicated partitioning system, but even then, some plasmid partitioning systems have been proposed to rely on an active diffusion-ratchet mechanism (Hwang et al., 2013; Vecchiarelli et al., 2013) in which plasmid diffusion is

an essential element. We even expect phages to be impacted by the physical nature of the cytoplasm, as the assembly of their genomes and capsids depends on their ability to interact.

Our data suggest that cellular metabolism fluidizes the cytoplasm, allowing larger cellular components to escape local environments and sample cytoplasmic space that they otherwise could not. This metabolism-induced fluidization may help the cell to achieve the delicate balance of attaining extremely high concentrations of biomolecules (to increase metabolism and cell proliferation) without severely compromising macromolecular motion. Ultimately, during the course of evolution, the glassy properties of the cytoplasm may have set upper limits to the size of molecular components and the degree of molecular crowding a cell can have. Higher crowding could result in particles of smaller sizes (such as proteins) "perceiving" the cytoplasm as more glass like, severely impacting biochemical reactions. Consistent with this idea, the mobility of free GFP becomes disproportionally reduced compared to a smaller molecule (e.g., glucose derivative) when high osmotic stress increases cytoplasmic crowding (Mika et al., 2010).

Another interesting outcome of the metabolic effect on cytoplasmic fluidity is that fluctuations in the environment can modulate cytoplasmic dynamics by affecting metabolism. Metabolic dormancy is widespread in the wild; for example, the fraction of quiescent cells ranges from 20% in the human gut to >80% in soil samples (Lennon and Jones, 2011). Dormancy has generated considerable interest in the scientific community, notably because of its links to both pathogenesis and antibiotic resistance (Coates, 2003). Dormancy is a survival strategy that bacteria in both environmental and clinical settings use to respond to stress such as starvation, antibiotic exposure, and high cell density (Lennon and Jones, 2011). We show that the motion of large components drops under metabolic depletion, and this occurs under natural conditions such as prolonged carbon starvation and late stationary phase (Figures 1B and 1C). This implies that the fluidity of the cytoplasm in dormant cells is very different compared to active cells, a difference that has not, to our knowledge, been considered. It would be interesting to examine in the future whether the vitrification of the dormant cytoplasm helps to preserve subcellular architecture during quiescent periods while still allowing diffusion of proteins and metabolites to permit a quick restart of growth when conditions improve.

EXPERIMENTAL PROCEDURES

Procedures used for imaging, strains construction, single-particle tracking, trajectory analysis, tracking precision estimation, image analysis, parameter determination (R_g, MSD, MSD_τ, α_2, γ), and particle size estimation are described in the Extended Experimental Procedures.

Strains, Plasmids, and Growth Conditions

A list of strains is provided in Table S1. Exponentially growing cell cultures were used in all experiments ($OD_{600} \leq 0.3$ for *E. coli* and $OD_{660} \leq 0.25$ for *C. crescentus*), except where noted.

C. crescentus strains were grown at 30°C in defined minimal M2G medium (Ely, 1991) and were supplemented with antibiotics when appropriate.

E. coli strain JP924 was grown at 30°C in M9 glycerol medium supplemented with casamino acids (M9G), 50 μg/ml of ampicillin, and 2 μg/ml of chloramphenicol. GFP-LacI expression was accomplished by spotting cells on agarose pads containing a concentration gradient of L-arabinose prior to imaging. CJW4386 (carrying *dnaC2*) was grown at 30°C in M9G, 50 μg/ml ampicillin, and 2 μg/ml chloramphenicol. Ninety minutes prior to imaging, the culture was shifted to 37°C, and L-arabinose was added (to a final concentration of 0.02%) 45 min prior to imaging.

E. coli strains CJW4617 and CJW4619 were grown at 30°C in M9G supplemented with 50 μg/ml kanamycin. GFP-μNS synthesis was induced by addition of isopropyl β-D-1-thiogalactopyranoside (IPTG) to 50–200 μM. After 30–120 min at 30°C, induction was stopped by washing cells into IPTG-free M9G medium. CJW4619 (carrying *dnaC2*) cells were incubated at 37°C for 2–3 hr to obtain filamentous cells.

Light Microscopy

Cells were imaged on agarose-padded slides supplemented with indicated media; see Extended Experimental Procedures for further details. Cell outlines were obtained from phase contrast images using open-source software MicrobeTracker (Sliusarenko et al., 2011). Fluorescent spots were detected and tracked using SpotFinder (Sliusarenko et al., 2011) and custom-built scripts in Matlab (The MathWorks), as described in the Extended Experimental Procedures.

SUPPLEMENTAL INFORMATION

Supplemental Information includes Extended Results, Extended Experimental Procedures, one table, and seven movies and can be found with this article online at http://dx.doi.org/10.1016/j.cell.2013.11.028.

ACKNOWLEDGMENTS

We are grateful to Jason Hocking for the construction of strains CJW4617 and CJW4619. We thank Dr. Anuradha Janakiraman, Dr. Max Nibert, and Dr. Cammie Lesser for providing the template for the construction of the IPTG-inducible allele that encodes GFP-μNS. We also thank Dr. Joe Pogliano for providing JP924 strain and Dr. Manuel Campos for sharing the information about nucleoid expansion in response to DNP treatment. We also thank all members of the Jacobs-Wagner lab for critical reading of the manuscript and for fruitful discussions. B.R.P. was, in part, supported by the National Institutes of Health (T32HG 003198). This work was supported by the National Institutes of Health (GM065835 to C.J.-W.). C.J.-W. is a Howard Hughes Medical Institute investigator.

Received: June 14, 2013
Revised: July 31, 2013
Accepted: November 5, 2013
Published: December 19, 2013

REFERENCES

Ausmees, N., Kuhn, J.R., and Jacobs-Wagner, C. (2003). The bacterial cytoskeleton: an intermediate filament-like function in cell shape. Cell *115*, 705–713.

Bakshi, S., Bratton, B.P., and Weisshaar, J.C. (2011). Subdiffraction-limit study of Kaede diffusion and spatial distribution in live Escherichia coli. Biophys. J. *101*, 2535–2544.

Berthier, L. (2011). Dynamic heterogeneity in amorphous materials. Physics *4*, 42.

Brangwynne, C.P., Koenderink, G.H., MacKintosh, F.C., and Weitz, D.A. (2009). Intracellular transport by active diffusion. Trends Cell Biol. *19*, 423–427.

Broering, T.J., Parker, J.S., Joyce, P.L., Kim, J., and Nibert, M.L. (2002). Mammalian reovirus nonstructural protein microNS forms large inclusions and colocalizes with reovirus microtubule-associated protein micro2 in transfected cells. J. Virol. *76*, 8285–8297.

Broering, T.J., Arnold, M.M., Miller, C.L., Hurt, J.A., Joyce, P.L., and Nibert, M.L. (2005). Carboxyl-proximal regions of reovirus nonstructural protein muNS necessary and sufficient for forming factory-like inclusions. J. Virol. *79*, 6194–6206.

Cabeen, M.T., Charbon, G., Vollmer, W., Born, P., Ausmees, N., Weibel, D.B., and Jacobs-Wagner, C. (2009). Bacterial cell curvature through mechanical control of cell growth. EMBO J. *28*, 1208–1219.

Cabeen, M.T., Murolo, M.A., Briegel, A., Bui, N.K., Vollmer, W., Ausmees, N., Jensen, G.J., and Jacobs-Wagner, C. (2010). Mutations in the Lipopolysaccharide biosynthesis pathway interfere with crescentin-mediated cell curvature in Caulobacter crescentus. J. Bacteriol. *192*, 3368–3378.

Cayley, S., Lewis, B.A., Guttman, H.J., and Record, M.T., Jr. (1991). Characterization of the cytoplasm of Escherichia coli K-12 as a function of external osmolarity. Implications for protein-DNA interactions in vivo. J. Mol. Biol. *222*, 281–300.

Cipelletti, L., and Ramos, L. (2005). Slow dynamics in glassy soft matter. J. Phys. Condens. Matter *17*, R253–R285.

Coates, A.R.M. (2003). Dormancy and low-growth states in microbial disease (Cambridge, New York: Cambridge University Press).

Coquel, A.S., Jacob, J.P., Primet, M., Demarez, A., Dimiccoli, M., Julou, T., Moisan, L., Lindner, A.B., and Berry, H. (2013). Localization of protein aggregation in Escherichia coli is governed by diffusion and nucleoid macromolecular crowding effect. PLoS Comp. Biol. *9*, e1003038.

Dawson, K.A. (2002). The glass paradigm for colloidal glasses, gels, and other arrested states driven by attractive interactions. Curr. Opin. Coll. Int. Sci. *7*, 218–227.

Derman, A.I., Lim-Fong, G., and Pogliano, J. (2008). Intracellular mobility of plasmid DNA is limited by the ParA family of partitioning systems. Mol. Microbiol. *67*, 935–946.

Dix, J.A., and Verkman, A.S. (2008). Crowding effects on diffusion in solutions and cells. Annu Rev Biophys *37*, 247–263.

Doliwa, B., and Heuer, A. (1998). Cage effect, local anisotropies, and dynamic heterogeneities at the glass transition: A computer study of hard spheres. Phys. Rev. Lett. *80*, 4915–4918.

Elowitz, M.B., Surette, M.G., Wolf, P.E., Stock, J.B., and Leibler, S. (1999). Protein mobility in the cytoplasm of Escherichia coli. J. Bacteriol. *181*, 197–203.

Ely, B. (1991). Genetics of Caulobacter crescentus. Methods Enzymol. *204*, 372–384.

English, B.P., Hauryliuk, V., Sanamrad, A., Tankov, S., Dekker, N.H., and Elf, J. (2011). Single-molecule investigations of the stringent response machinery in living bacterial cells. Proc. Natl. Acad. Sci. USA *108*, E365–E373.

Fabry, B., Maksym, G.N., Butler, J.P., Glogauer, M., Navajas, D., and Fredberg, J.J. (2001). Scaling the microrheology of living cells. Phys. Rev. Lett. *87*, 148102.

Fehr, T., and Löwen, H. (1995). Glass transition in confined geometry. Phys. Rev. E *52*, 4016–4025.

Golding, I., and Cox, E.C. (2006). Physical nature of bacterial cytoplasm. Phys. Rev. Lett. *96*, 098102.

Heun, P., Laroche, T., Shimada, K., Furrer, P., and Gasser, S.M. (2001). Chromosome dynamics in the yeast interphase nucleus. Science *294*, 2181–2186.

Hunter, G.L., and Weeks, E.R. (2012). The physics of the colloidal glass transition. Rep. Prog. Phys. *75*, 066501.

Hwang, L.C., Vecchiarelli, A.G., Han, Y.W., Mizuuchi, M., Harada, Y., Funnell, B.E., and Mizuuchi, K. (2013). ParA-mediated plasmid partition driven by protein pattern self-organization. EMBO J. *32*, 1238–1249.

Jun, S., and Wright, A. (2010). Entropy as the driver of chromosome segregation. Nat. Rev. Microbiol. *8*, 600–607.

Kegel, W.K., and van Blaaderen, A. (2000). Direct observation of dynamical heterogeneities in colloidal hard-sphere suspensions. Science *287*, 290–293.

Latulippe, D.R., and Zydney, A.L. (2010). Radius of gyration of plasmid DNA isoforms from static light scattering. Biotechnol. Bioeng. *107*, 134–142.

Lennon, J.T., and Jones, S.E. (2011). Microbial seed banks: the ecological and evolutionary implications of dormancy. Nat. Rev. Microbiol. *9*, 119–130.

Levi, V., Ruan, Q., Plutz, M., Belmont, A.S., and Gratton, E. (2005). Chromatin dynamics in interphase cells revealed by tracking in a two-photon excitation microscope. Biophys. J. *89*, 4275–4285.

Maehara, A., Taguchi, S., Nishiyama, T., Yamane, T., and Doi, Y. (2002). A repressor protein, PhaR, regulates polyhydroxyalkanoate (PHA) synthesis via its direct interaction with PHA. J. Bacteriol. *184*, 3992–4002.

Marcus, A.H., Schofield, J., and Rice, S.A. (1999). Experimental observations of non-Gaussian behavior and stringlike cooperative dynamics in concentrated quasi-two-dimensional colloidal liquids. Phys. Rev. E *60* (5 Pt B), 5725–5736.

Mika, J.T., van den Bogaart, G., Veenhoff, L., Krasnikov, V., and Poolman, B. (2010). Molecular sieving properties of the cytoplasm of Escherichia coli and consequences of osmotic stress. Mol. Microbiol. *77*, 200–207.

Montero Llopis, P., Sliusarenko, O., Heinritz, J., and Jacobs-Wagner, C. (2012). In vivo biochemistry in bacterial cells using FRAP: insight into the translation cycle. Biophys. J. *103*, 1848–1859.

Nenninger, A., Mastroianni, G., and Mullineaux, C.W. (2010). Size dependence of protein diffusion in the cytoplasm of Escherichia coli. J. Bacteriol. *192*, 4535–4540.

Niu, L., and Yu, J. (2008). Investigating intracellular dynamics of FtsZ cytoskeleton with photoactivation single-molecule tracking. Biophys. J. *95*, 2009–2016.

Petekidis, G., Moussaïd, A., and Pusey, P.N. (2002). Rearrangements in hard-sphere glasses under oscillatory shear strain. Phys. Rev. E Stat. Nonlin. Soft Matter Phys. *66*, 051402.

Pusey, P.N., and van Megen, W. (1986). Phase-behavior of concentrated suspensions of nearly hard colloidal spheres. Nature *320*, 340–342.

Qi, Q.S., and Rehm, B.H.A. (2001). Polyhydroxybutyrate biosynthesis in Caulobacter crescentus: molecular characterization of the polyhydroxybutyrate synthase. Microbiology *147*, 3353–3358.

Sliusarenko, O., Heinritz, J., Emonet, T., and Jacobs-Wagner, C. (2011). High-throughput, subpixel precision analysis of bacterial morphogenesis and intracellular spatio-temporal dynamics. Mol. Microbiol. *80*, 612–627.

Soutoglou, E., and Misteli, T. (2007). Mobility and immobility of chromatin in transcription and genome stability. Curr. Opin. Genet. Dev. *17*, 435–442.

Spitzer, J. (2011). From water and ions to crowded biomacromolecules: in vivo structuring of a prokaryotic cell. Microbiol. Mol. Biol. Rev. *75*, 491–506.

Spitzer, J., and Poolman, B. (2009). The role of biomacromolecular crowding, ionic strength, and physicochemical gradients in the complexities of life's emergence. Microbiol. Mol. Biol. Rev. *73*, 371–388.

Swaminathan, R., Hoang, C.P., and Verkman, A.S. (1997). Photobleaching recovery and anisotropy decay of green fluorescent protein GFP-S65T in solution and cells: cytoplasmic viscosity probed by green fluorescent protein translational and rotational diffusion. Biophys. J. *72*, 1900–1907.

Vecchiarelli, A.G., Hwang, L.C., and Mizuuchi, K. (2013). Cell-free study of F plasmid partition provides evidence for cargo transport by a diffusion-ratchet mechanism. Proc. Natl. Acad. Sci. USA *110*, E1390–E1397.

Weber, S.C., Spakowitz, A.J., and Theriot, J.A. (2010). Bacterial chromosomal loci move subdiffusively through a viscoelastic cytoplasm. Phys. Rev. Lett. *104*, 238102.

Weber, S.C., Spakowitz, A.J., and Theriot, J.A. (2012). Nonthermal ATP-dependent fluctuations contribute to the in vivo motion of chromosomal loci. Proc. Natl. Acad. Sci. USA *109*, 7338–7343.

Weeks, E.R., and Weitz, D.A. (2002). Properties of cage rearrangements observed near the colloidal glass transition. Phys. Rev. Lett. *89*, 095704.

Weeks, E.R., Crocker, J.C., Levitt, A.C., Schofield, A., and Weitz, D.A. (2000). Three-dimensional direct imaging of structural relaxation near the colloidal glass transition. Science *287*, 627–631.

Zaccarelli, E., Mayer, C., Asteriadi, A., Likos, C.N., Sciortino, F., Roovers, J., Iatrou, H., Hadjichristidis, N., Tartaglia, P., Löwen, H., and Vlassopoulos, D. (2005). Tailoring the flow of soft glasses by soft additives. Phys. Rev. Lett. *95*, 268301.

Zimmerman, S.B., and Trach, S.O. (1991). Estimation of macromolecule concentrations and excluded volume effects for the cytoplasm of *Escherichia coli*. J. Mol. Biol. *222*, 599–620.